

Article

Design and Experiments of a Galloping-Based Wind Energy Harvester Using Quadruple Halbach Arrays

Hai Dang Le  and Soon-Duck Kwon * 

Department of Civil Engineering, Jeonbuk National University, Jeonju 54896, Jeonbuk, Korea; lhdang@jbnu.ac.kr
* Correspondence: sdkwon@jbnu.ac.kr

Abstract: This study aims to develop a device for harvesting electrical energy from low-speed natural wind. Four linear Halbach arrays are adopted to design a high-performance galloping harvester with the advantage of high durability and efficiency at low-frequency vibrations. The results of magnetic field analysis reveal that there are optimal sizes of the main and transit magnets of the Halbach arrays and coil to obtain the maximum magnetic flux density normal to the coil. The experimental and simulation results show that the electrical external load resistance significantly affects the vibration amplitude and the galloping onset velocity of the harvester. The results also reveal that the performance of the original design using the quadruple Halbach array was lower than that of the existing harvester because of the heavy magnet mass embedded in the tip prism. The modified design, reducing mass, improved the performance by four times compared to the original design.

Keywords: energy harvest; wind; galloping; Halbach array; electromagnetic



Citation: Le, H.D.; Kwon, S.-D. Design and Experiments of a Galloping-Based Wind Energy Harvester Using Quadruple Halbach Arrays. *Energies* **2021**, *14*, 6094. <https://doi.org/10.3390/en14196094>

Academic Editor: Antonio Crespo

Received: 29 August 2021
Accepted: 21 September 2021
Published: 24 September 2021

Publisher's Note: MDPI stays neutral with regard to jurisdictional claims in published maps and institutional affiliations.



Copyright: © 2021 by the authors. Licensee MDPI, Basel, Switzerland. This article is an open access article distributed under the terms and conditions of the Creative Commons Attribution (CC BY) license (<https://creativecommons.org/licenses/by/4.0/>).

1. Introduction

Most wireless sensors are currently powered by batteries, which require regular charging or replacement. Owing to the high cost and inconvenience of battery replacement, powering wireless sensor systems by energy harvesters has been developing rapidly and has shown great achievements in many different applications. There have been many studies to develop energy harvesters based on piezoelectric [1–3], electromagnetic [4–6], and electrostatic [7] transductions.

Electrostatic harvesters are compact converters with a simple structure. However, electrostatic generators convert less power per unit volume than piezoelectric generators [7]. Piezoelectric generators also have a compact configuration and produce high-output voltage. However, the drawbacks of piezoelectric generators are low durability under repeated stress and low efficiency at low frequency. Electromagnetic generators are highly durable and are efficient at low frequency. However, they generate a low output voltage and are bulky in size due to their magnets and pick-up coil.

Wind is a widespread kinetic energy readily available in nature. However, small generators that have been scaled down from proven large wind turbines have poor performance due to aerodynamic problems, such as high drag at low Reynolds numbers. Therefore, successful miniature wind energy harvesters use fluid-induced vibrations such from galloping [4,5], flutter [3,8] vortex-induced vibration [9,10], and wake galloping [11].

Flutter, a divergent vibration, is a good energy source because of its large amplitude. However, there is a disadvantage that flutter does not occur easily in low natural winds due to its high onset velocity. Vortex-induced vibration occurs only in the lock-in range where the vortex shedding frequency becomes close to the natural frequency of the harvester. Therefore, the main drawback of vortex-induced vibration harvester is the narrow bandwidth of wind speed for generating electric power. Zhao and Yang [12] provided an intensive literature review of wind energy harvesters.

Galloping is a widely used wind energy source because it readily occurs at low wind speeds. Galloping of an elastic body occurs when the wind speed exceeds a certain threshold, resulting in a significantly large oscillation [13]. Many researchers have proposed energy harvesters to convert aeroelastic galloping vibrations into electricity [4,5,12–17]. A galloping energy harvester generally consists of a tip prism to generate a galloping aerodynamic instability, a metal cantilever or spring that provides a restoring force, and a generator that converts vibrations into electricity. The performance of a galloping energy harvester depends on how well the electric generator is designed to cope with aerodynamic instability.

In order to take advantage of electromagnetic transduction suitable for low-frequency, wind-induced vibrations, Le and Kwon [4] proposed a cantilever-type galloping energy harvester with a double magnet design. This study aims to propose a new energy harvester design by adopting Halbach arrays to increase the magnetic flux. The new harvester is investigated through theoretical and experimental studies. The scope of this study is limited to the design of an electromagnetic generator associated aerodynamic galloping phenomena, and does not deal with charging or related electrical issues.

2. Method and Analysis

2.1. Device Configuration

A galloping energy harvester is a device that generates a modest amount of electricity using wind-induced vibration. Figure 1 shows a schematic of a typical galloping energy harvester, which primarily consists of a tip prism, a cantilever plate, and an electric generator. The movable tip prism elicits aerodynamic galloping instability, and the cantilever plate or spring provides a restoring force. Piezoelectric or electromagnetic generators are commonly used. A piezoelectric generator converts the bending strain at the cantilever root, but is less durable under repeated vibrations. An electromagnetic generator uses relative motion between the magnet and the coil, which is produced by galloping.

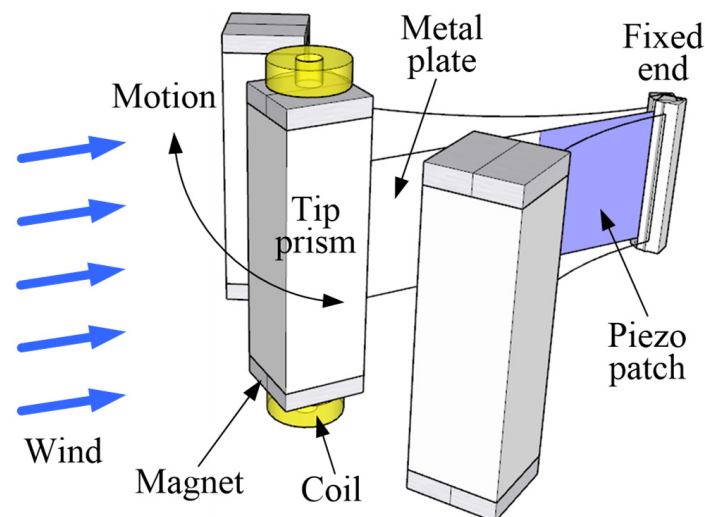


Figure 1. Schematic of a typical galloping energy harvester.

Galloping, a well-known aerodynamic instability, is the main energy source for power generation here. There are three main considerations for designing a high-performance galloping harvester. First, the shape of the tip prism should be designed to easily facilitate galloping. It is known that galloping occurs severely in square cross-section [18,19]. Second, the mechanical damping of the harvester must be as low as possible to generate high-amplitude oscillations at low wind speeds. A cantilever structure is advantageous in reducing the mechanical damping because there are few friction-causing links or connections in cantilever. Third, the electric generator must be designed considering the interaction with the aerodynamic vibration; too much electrical generation results in lower

galloping amplitudes and higher cut-in wind speeds. The balance between generated electric power with galloping-driven power is important.

The induced current of an electromagnetic generator is proportional to the magnetic flux density. The higher the magnetic flux density, the higher the performance of the generator. Unlike ordinary magnets, a Halbach array has asymmetrical magnetic fields. As shown in Figure 2, the Halbach array consists of main magnets and transit magnets. The superimposition of the magnetic flux caused by main magnets and transit magnets creates a stronger magnetic field on the active side while reducing the field on the quiet side to near zero. The coil placed on the active side can receive a stronger magnetic flux.

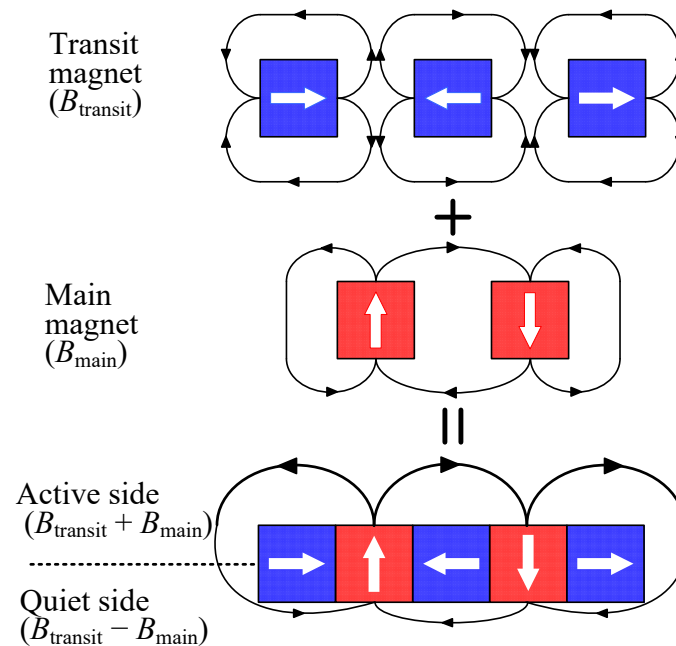


Figure 2. Principle of the Halbach arrays magnetic circuits [20].

There are a few types of Halbach arrays depending on the magnet arrangement, such as linear, cylindrical, and spherical arrays. One of the main disadvantages of Halbach arrays is the difficulty in forming the target arrangement because of strong repulsive magnetic forces. This makes Halbach arrays expensive to fabricate. However, the flat linear Halbach arrays have a simple structure and are cost-effective compared with other arrangements.

This study employs multiple linear Halbach arrays to increase the magnetic flux density at the coil. Figure 3 shows a schematic of the generator proposed in this study. Two linear Halbach arrays composed of five magnets each are placed on both sides, and a pick-up coil is placed between them. By placing the two Halbach arrays facing each other, the magnetic flux is concentrated on the inside where the coil is located and the magnetic flux is low on the outside.

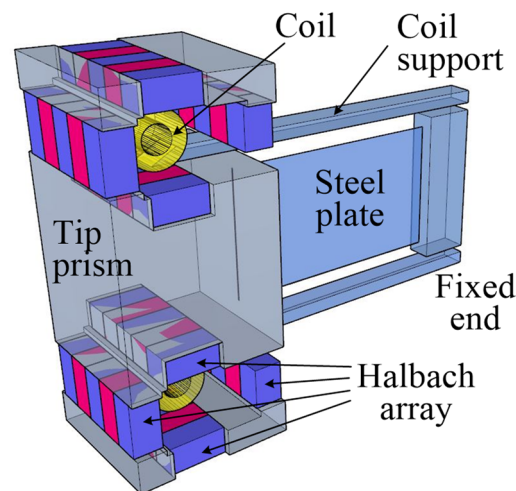


Figure 3. Schematic of the proposed energy harvester with Halbach arrays (red: main magnet, blue: transit magnet).

2.2. Basic Theory

The response of a galloping energy harvester is governed by the fluid–structure–electromagnetic interaction. When a damped-prism oscillator is subjected to a crosswind force and an electromagnetic force, the governing equation can be expressed as:

$$m\ddot{y}(t) + c\dot{y}(t) + ky(t) = F_{wind}(t) + F_{em}(t) \quad (1)$$

where y is the tip displacement, m is the mass, c is the mechanical damping coefficient, k is the stiffness provided by the cantilever or spring, F_{wind} is the wind force, and F_{em} is the electromagnetic force induced by the coil. The relation between the induced coil voltage and the relative velocity between the coil and the magnet is given by:

$$\dot{V}(t) + \frac{(R_L + R_c)}{L_c}V(t) = \Phi(t)\frac{R_L}{L_c}\dot{y}(t) \quad (2)$$

where V is the generated voltage, R_c is the coil resistance, R_L is the external load resistance, L_c is the coil inductance, and Φ is the electromechanical coupling coefficient related to the magnetic field. The following approximation is applicable to estimate the average coupling coefficient of the coil [21] as:

$$\Phi \approx B_n l_w \quad (3)$$

where B_n is the average normal component of the magnetic flux density to the coil, and l_w is the total coil length in the magnetic field. The electromagnetic forces opposing the vibrational motion can be described as a function of the induced voltage in the coil as:

$$F_{em} = \frac{\Phi(t)}{R_L}V(t) \quad (4)$$

The attitude of the galloping body with respect to the flow depends on the wind velocity and the moving body velocity. The rotation angle of the tip prism also affects the resultant wind velocity. The effective angle of attack at the tip can be derived from a quasi-steady approach, considering the wind velocity, body velocity, and the tip rotation angle. The wind force acting on the tip prism is given by Equation (5):

$$F_{wind} = \frac{1}{2}\rho U^2 A \left\{ a_1 \left(\frac{\dot{y}(t)}{U} - \frac{3y(t)}{2L} \right) + a_3 \left(\frac{\dot{y}(t)}{U} - \frac{3y(t)}{2L} \right)^3 \right\} \quad (5)$$

where U is the wind speed, ρ is the air density, A is the frontal area of the tip prism, L is the cantilever length, and a_1 and a_3 are the empirical galloping coefficients associated with shape of the tip prism. The generated electric power is obtained from the voltage and the applied external load resistance using the following relation:

$$P \approx V^2/R_L \quad (6)$$

2.3. Simulation Model

For the analysis and design of this galloping energy harvester, the analysis was divided into two stages. First, the magnetic flux density acting on the coil was calculated to optimize the performance of the electromagnetic generator. These computations were performed using FEMM 4.2 software [22].

Then an analysis was done to obtain the dynamic displacement and the induced voltage of the galloping energy harvester by simultaneously solving Equations (1) and (2); the results were nonlinear because of the cubic power terms related to the angle of attack in Equation (5). The Runge-Kutta 4th order method in MATLAB was used in the simulation.

3. Design Optimization

3.1. Optimization of the Magnet and Coil Dimensions

As shown in Figure 3, two electric generators were placed at the top and bottom of the tip prism. Each generator consisted of a linear Halbach array and a pick-up coil, as shown in Figures 2 and 4. The relative size and position of the coil and magnets affected the performance of the generator. Figure 4 shows the main parameters for optimization: the sizes of the main magnet and the transit magnet, and the width and height of the coil.

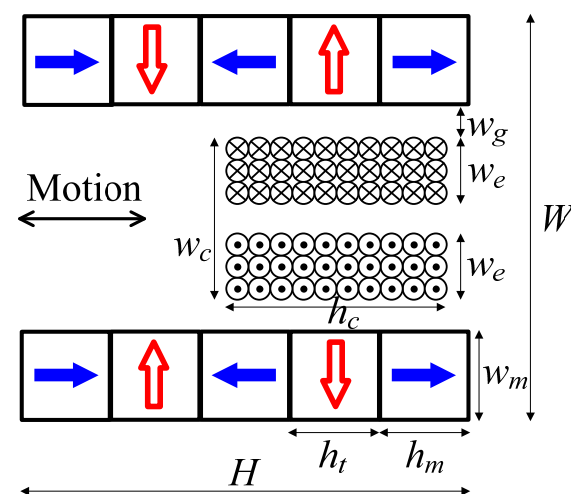


Figure 4. Optimization parameters for linear Halbach arrays and pick-up coils (⇨: main magnet and pole direction, ⇨: transit magnet and pole direction).

As shown in Equations (2) and (3), the induced voltage in the coil is proportional to the magnetic flux density and the relative velocity between the coil and the magnets. Assuming that the amplitude of the galloping is consistent, the amount of generated electric power is proportional to the magnetic flux density where the coil is located. In order to optimize the performance of the generator, the finite element method (in the FEMM 4.2 software) was used to investigate the magnetic flux density according to the relative size of the magnet and the coil. Only the normal component of magnetic flux to the coil was used for comparison.

Each magnet in the linear Halbach arrays consisted of rare-earth neodymium, iron, and boron (NdFeB). The dimensions of each magnet were initially set as 10 mm × 10 mm, and the width of the gap for the free movement of the magnet and the coil was set to be 1 mm. For relative comparison, the sizes of the magnets and coils were normalized by

dividing the reference dimensions. Figure 5 shows the results of magnetic field analysis around the Halbach arrays.

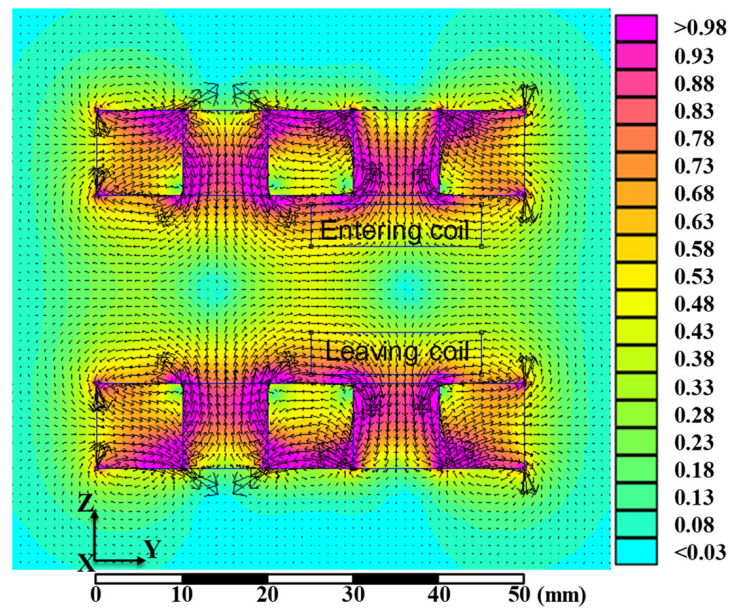


Figure 5. Magnetic flux density (Tesla) around the linear Halbach arrays.

3.2. Magnetic Flux Density Normal to the Coil

Figure 6 shows the change of magnetic flux density that is normal to the coil according to the ratio of the main magnet width to the coil width. As the width ratio increases, the magnetic flux density also increases and then decreases. The magnetic flux density is at its maximum when the width of the main magnet is twice the width of the coil.

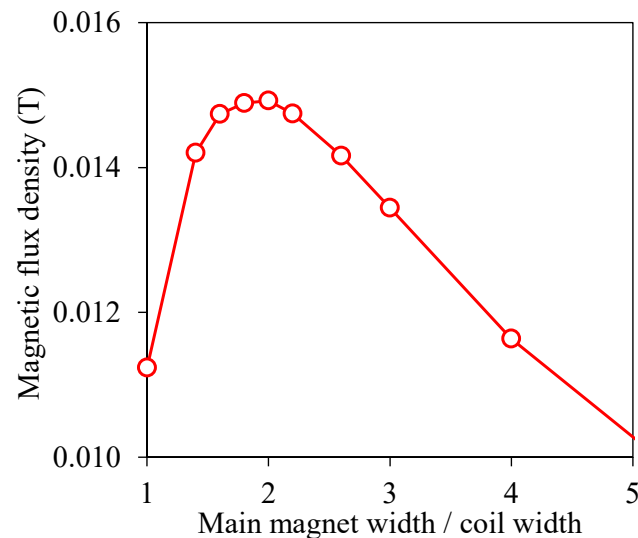


Figure 6. Variation of magnetic flux density according to the ratio of the main magnet width (w_m) to the coil width (w_c).

Figure 7 shows the change of magnetic flux density normal to the coil according to the ratio of the coil height to the main magnet height. It is assumed that the height of the main magnet and the transit magnet is the same. As the height ratio increases, the magnetic flux density also increases and then decreases slightly. When the coil height is twice the height of the main magnet, the magnetic flux density is at its maximum.

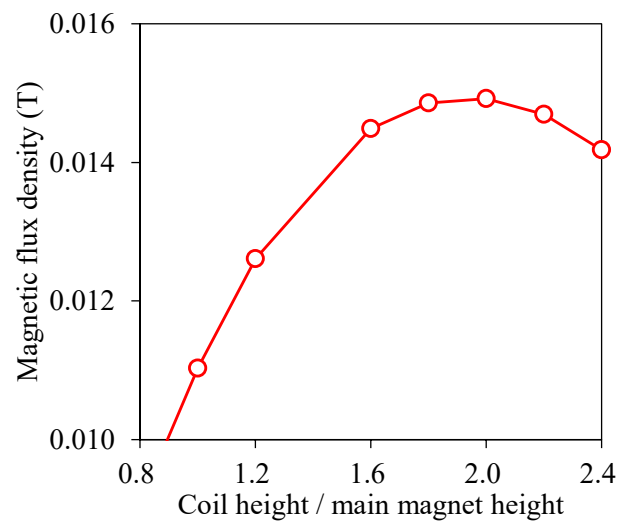


Figure 7. Variation of magnetic flux density according to the ratio of the coil height (h_c) to the main magnet height (h_m).

Figure 8 shows the change of magnetic flux density as a function of the ratio of the main magnet height to the transit magnet height. The magnetic flux density of the coil is maximized when the heights of the main and transit magnets are equal.

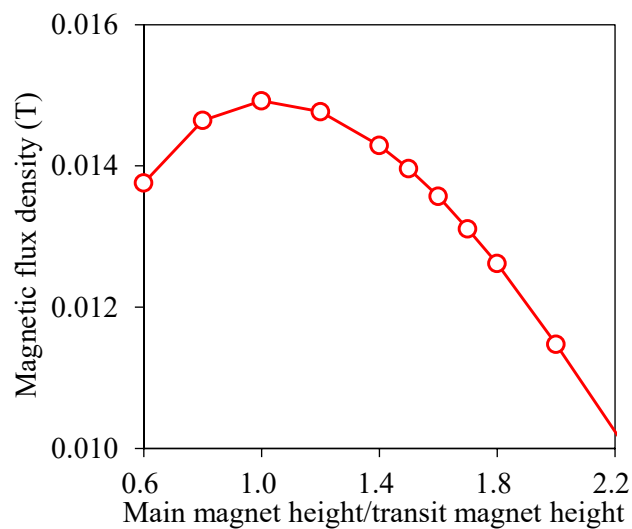


Figure 8. Variation of magnetic flux density according to the ratio of the main magnet height (h_m) to the transit magnet height (h_t).

3.3. Prototype Device

Figure 9 shows the prototype galloping energy harvester, including the generator. The final design of the generator is in the form of a coil surrounded by four Halbach arrays. Note that the coils are separately fixed but the Halbach arrays embedded at both ends of the tip prism are movable. In Figure 3, if only the left and right Halbach arrays are removed, or the upper and lower Halbach arrays are removed, the arrangement of coils and magnets is the same as that in Figure 4. Since the four Halbach arrays are arranged to face each other two-by-two, the results of the parameter studies in the previous section can be applied as-is. In addition, this design using four units saves generator space and increases the magnetic flux density.

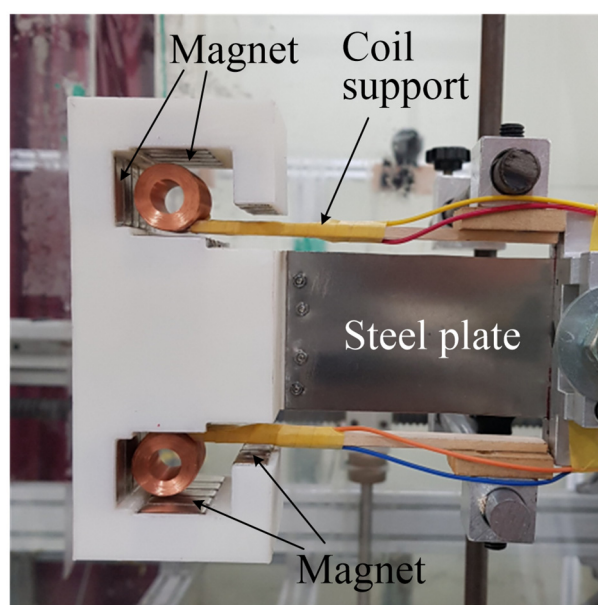


Figure 9. Prototype of the proposed galloping energy harvester with four Halbach arrays.

The steps to design this prototype galloping energy harvester were: First, determine the dimensions of the electromagnetic generator, which consists of magnets and coils. Second, determine the shape and size of the tip prism that has a built-in generator and generates vibration by galloping. Third, determine the natural frequency corresponding to the target cut-in wind speed and the associated cantilever dimensions.

The optimal magnet and coil sizes were determined from the parametric study. In practical terms, the size of the magnets was selected according to commercial availability, even though it was slightly different from optimal. The dimensions of each magnet in the Halbach arrays were 10 mm (wide) \times 10 mm (high) \times 20 mm (long). Each Halbach array was made up of five identical neodymium magnets (NdFeB) of N35 grade, and the resulting size was 10 mm (wide) \times 50 mm (high) \times 20 mm (long). The parameters of the single coil are detailed in Table 1. The gap between the magnet and the coil was 2 mm.

Table 1. Parameters of a single coil.

Parameter	Quantity
Wire gauge	38 AWG
Outer diameter	20 mm
Inner diameter	10 mm
Length	20 mm
Number of turns	7400
Resistance	787 Ω
Inductance	432 mH

The tip prism was basically square cylinder with open spaces for coil and support that was made by 3D printer. The cross section of the 132-mm-long tip prism was 55 mm \times 55 mm, which was slightly larger than the Halbach array. The mass of the tip prism (including the magnets) was 641 g. The size of the steel cantilever plate was 50 mm (wide) \times 0.4 (thick) \times 86 (long). This device was supported by only a thin stainless steel plate, resulting inherently low mechanical damping.

4. Experimental Verification

4.1. Experimental Setup

During the wind tunnel, it was not necessary to correct the experimental results because the blockage ratio was less than 1%. A pitot tube and an anemometer (FC012; Furness Controls, East Sussex, UK) were used to measure the wind speed in the tunnel. The tip displacements were measured from images acquired by a camera through an image processing technique. The output voltage was monitored on a digital multimeter (34410A; Agilent, Santa Clara, CA, USA), and was converted into power from the output voltage and the applied electrical load resistance using the relation in Equation (6).

The open circuit natural frequency and the damping ratio of the harvester were 1.807 Hz and 0.4%, respectively. The two coils at the upper and lower tip were connected in series. The electro-mechanical coupling coefficient in Equation (2) was determined by the free vibration test, wherein the tip prism was simply moved back and released, and then the tip displacement and the induced voltage were simultaneously measured. The electro-mechanical coupling coefficient was obtained as a function of the relative position between the coil and the magnet by dividing the voltage by the moving velocity.

After conducting a preliminary wind tunnel test, it was found that the empirical galloping coefficients for the square prisms in multiple references [15,16,23] were not applicable to the proposed device. The present harvester is not a complete square cylinder because of the coil spaces in the tip prism and the supporting cantilever plate. Therefore, the galloping coefficients were obtained from the re-analysis of Equations (1) and (5) compared with the experimental responses. The a_1 and a_3 values for the present device were 3.0 and -3.3 , respectively, in a Reynolds number range of 10,300–41,300.

4.2. Results

Figures 10 and 11 show the tip displacement and the average electric power as functions of wind velocity and electrical external load resistance. There were some differences between the measured and simulated results, possibly caused by the simple galloping coefficients used in the simulation not properly simulating the aerodynamic behavior of the complex shape of the harvester. It is clear from the figures that the electrical load resistance significantly affected the vibration amplitude and the galloping onset speed of the harvester by dissipating energy. Evidently, the cut-in wind velocity gradually moved to higher values as the load resistance decreased.

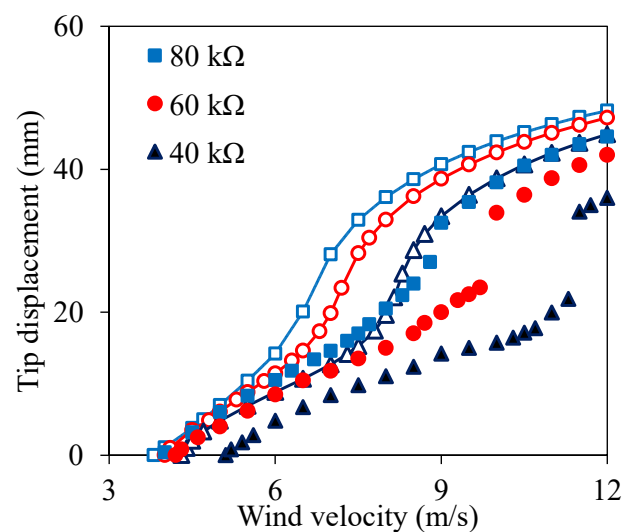


Figure 10. Variation of the tip displacements with wind velocity for different external load resistances (solid symbols: measured; lines with empty symbols: simulated).

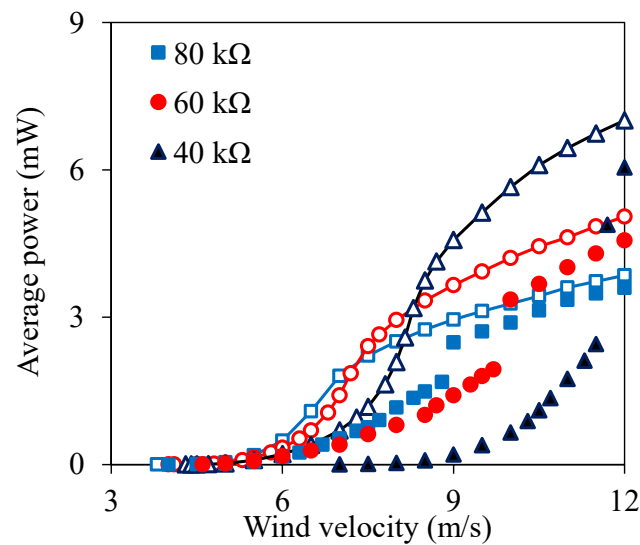


Figure 11. Variation of the average (RMS) power with wind velocity for different external load resistances (solid symbols: measured; lines with empty symbols: simulated).

When the galloping was fully developed, more electricity could be harvested at low external resistance. However, the high additional electrical damping due to the low external resistance increased the cut-in wind velocity, so that electricity could not be harvested at low wind speed. The trade-off between the generated electric power and the cut-in wind speed needs to be balanced.

Figures 12 and 13 show the measured and simulated average voltage and power versus external load resistances at three different wind velocities. When the load resistance gradually increased, the average voltage dramatically increased and then converged to a certain value, whereas the average power initially increased until its maximum value and then decreased. The external load resistances at which the voltage converged were equal to those for the maximum powers. The average power was very sensitive to external load resistance. The optimum load resistance for obtaining the maximum power was not constant—it varied with the wind speed.

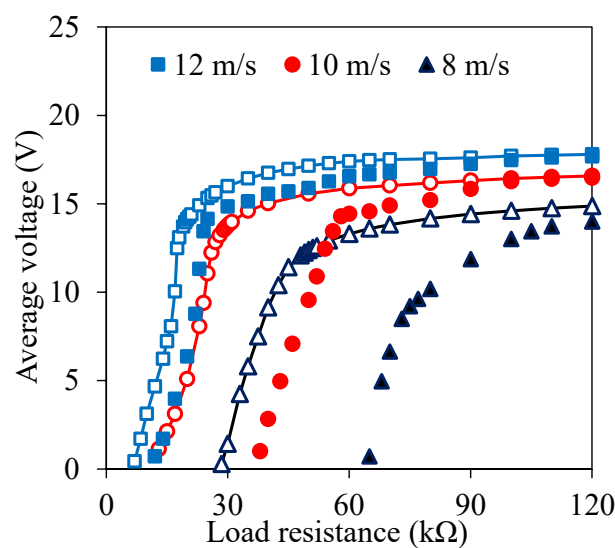


Figure 12. Variation of the average (RMS) voltage with the external load resistance for different wind velocities (solid symbols: measured; lines with empty symbols: simulated).

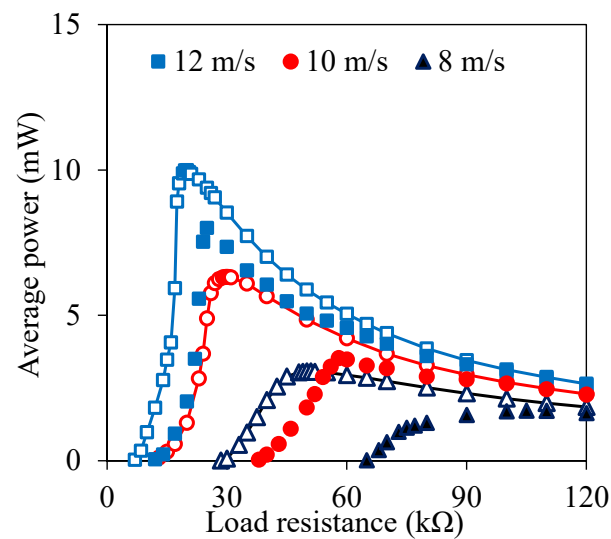


Figure 13. Variation of the average (RMS) power with the external load resistance for different wind velocities (solid symbols: measured; lines with empty symbols: simulated).

Figure 14 shows the strong coupling between the galloping onset velocity and the external load resistance as a result of higher electric damping. The results revealed that one specific load resistance should not be applied to the entire wind speeds; rather, it should be changed according to the wind speed in order to produce the maximum power.

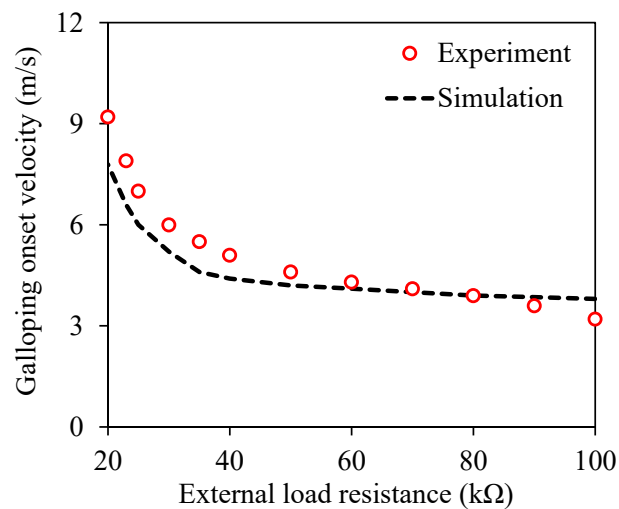


Figure 14. Variation of the galloping onset wind velocity with external load resistances.

Figure 15 shows the optimal external resistance to obtain the maximum average power for each wind speed. As the wind speed and associated fluid energy increased, the optimal external load resistance inversely decreased and more energy could be harvested. Figure 16 shows the maximum average power that could be obtained with the optimal external resistance. This harvester could obtain power from a low wind speed if the external resistance was properly adjusted, and 8 mW of power could be obtained at a wind speed of 12 m/s.

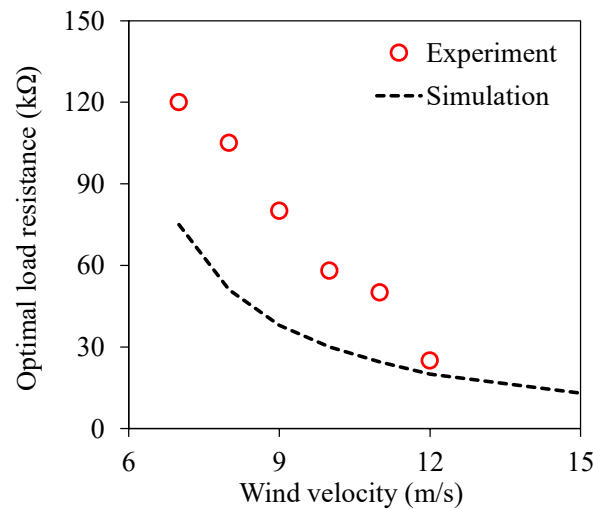


Figure 15. Variation of the optimal external load resistance with wind velocity.

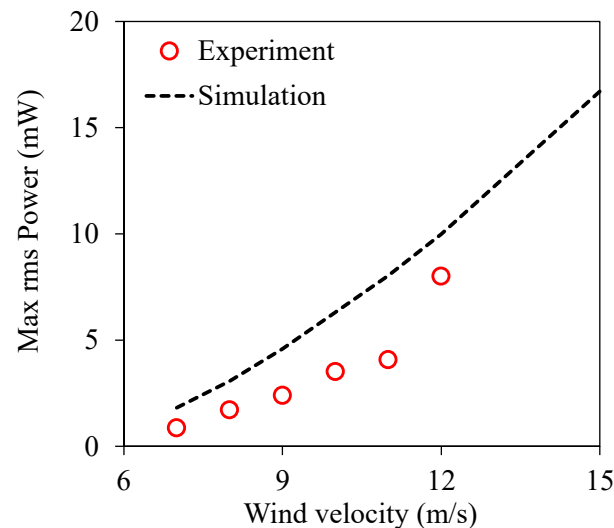


Figure 16. Variation of the maximum average (RMS) power with wind velocity under optimal load resistance.

4.3. Modified Design

Figure 17 compares the performance of the Le and Kwon [4] and the harvester of the original design using the Halbach array. The performance of the original design is lower than that of the previous one. The main reason for the low performance of the original design is the heavy mass of the tip prism. The tip mass of the original design was 641 g, but the mass of the previous one was 60 g, a significant difference. Embedded Halbach magnets in the tip prism significantly increased the mass. As the mass of the original design increased, the galloping wind speed increased and the amplitude decreased, reducing power production.

The harvester design was modified to solve the mass problem. As shown in Figure 3, in the original design, the magnets were embedded in the tip prism, and the coil was held in place by a separate support. Conversely in the modified design, the coil was embedded in the tip prism and the magnet was supported separately. As the magnets were separated from the tip prism, the tip mass was reduced to 113 g in the modified design. Figure 17 shows the maximum average power density of the previous harvester, the original design and the modified design. The results were obtained from numerical analysis. In the analysis, the properties of the original and modified designs were the same except for the mass. The power density was obtained by dividing the volume of the

rectangular prism containing the device. By reducing the tip mass in the modified design, the galloping wind speed was lowered to about 1 m/s, and the power density improved by a factor of 4 compared to the original design. The modified design was still similar in performance to the previous harvester, so there was no significant improvement.

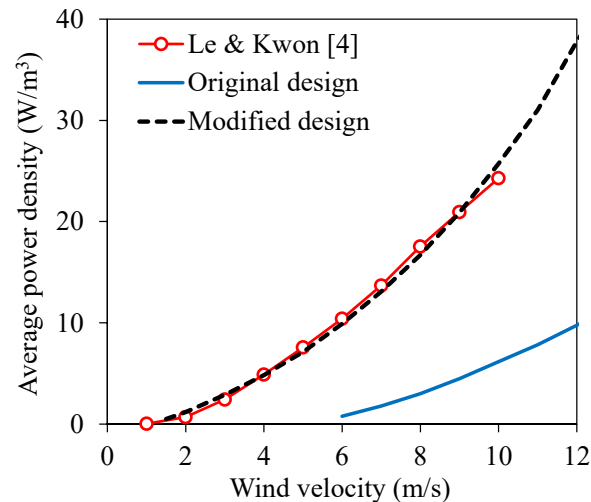


Figure 17. Maximum average power density under optimal load resistance obtained from numerical analysis.

Due to difficulties in manufacturing quadruple Halbach arrays, the gap between the coil and the magnet was widened to more than 2 mm. One of the four Halbach arrays was further spaced apart in order to secure a space for the support to pass through. For this reason, the performance of the prototype harvester was lower than the performance predicted during the optimization process. A more precise fabrication of the quadruple Halbach array parts has the potential to improve the performance of the harvester over the modified design.

5. Conclusions

This study develops a galloping-based wind energy harvester with quadruple Halbach arrays. The size of the main magnets and transit magnets in each Halbach array, and the associated width and height of the coil, are optimized from a magnetic field analysis. The magnetic flux density normal to the coil was at maximum when the heights of the main and transit magnets were the same, the width of the main magnet was twice the width of the coil, and the height of the main magnet was half the height of the coil.

From the wind tunnel test and numerical simulation of the prototype harvester, it was found that the electrical external load resistance significantly affected the vibration amplitude and the galloping onset velocity of the harvester. The results also revealed that one specific external load resistance should not be applied to the entire wind speeds, but, rather, should be changed according to the wind speed for producing the maximum power.

The test and analysis reveal that the performance of the original design harvester using the quadruple Halbach array was lower than that of the existing harvester [4]. The main reason for the low performance of the original design is the heavy mass caused by the embedded Halbach magnets in the tip prism. A modified design was proposed in which the tip mass was reduced by exchanging the support of the magnet and the coil. The modified design improved the maximum average power density by four times compared to the original design, and the performance was comparable to that of the existing harvester. It was predicted that the magnetic flux density would increase in the harvester using the Halbach arrays, but there was no significant performance improvement due to manufacturing difficulties. A more precise fabrication of the quadruple Halbach array parts has the potential to further improve the performance.

Author Contributions: Conceptualization, H.D.L., S.-D.K.; methodology, S.-D.K.; software, validation and formal analysis, H.D.L.; data curation, S.-D.K.; writing-original draft preparation, H.D.L.; writing-review and editing, S.-D.K.; supervision, S.-D.K. All authors have read and agreed to the published version of the manuscript.

Funding: This research was supported by the Basic Science Research Program through the National Research Foundation of Korea (NRF) funded by the Ministry of Education (No. 2017R1D1A3B03030206). This paper was also supported by research funds of Jeonbuk National University in 2019.

Conflicts of Interest: The authors declare no conflict of interest.

References

1. Anton, S.R.; A Sodano, H. A review of power harvesting using piezoelectric materials (2003–2006). *Smart Mater. Struct.* **2007**, *16*, R1–R21. [[CrossRef](#)]
2. Elahi, H.; Eugeni, M.; Gaudenzi, P. A Review on Mechanisms for Piezoelectric-Based Energy Harvesters. *Energies* **2018**, *11*, 1850. [[CrossRef](#)]
3. Kwon, S.-D. A T-shaped piezoelectric cantilever for fluid energy harvesting. *Appl. Phys. Lett.* **2010**, *97*, 164102. [[CrossRef](#)]
4. Le, H.D.; Kwon, S.-D. An electromagnetic galloping energy harvester with double magnet design. *Appl. Phys. Lett.* **2019**, *115*, 133901. [[CrossRef](#)]
5. Zhang, L.; Dai, H.; Abdelkefi, A.; Lin, S.; Wang, L. Theoretical modeling, wind tunnel measurements, and realistic environment testing of galloping-based electromagnetic energy harvesters. *Appl. Energy* **2019**, *254*, 113737. [[CrossRef](#)]
6. Liu, X.; Qiu, J.; Chen, H.; Xu, X.; Wen, Y.; Li, P. Design and Optimization of an Electromagnetic Vibration Energy Harvester Using Dual Halbach Arrays. *IEEE Trans. Magn.* **2015**, *51*, 1–4. [[CrossRef](#)]
7. Roundy, S.; Wright, P.K.; Rabaey, J. A study of low level vibrations as a power source for wireless sensor nodes. *Comput. Commun.* **2003**, *26*, 1131–1144. [[CrossRef](#)]
8. Bao, C.; Dai, Y.; Wang, P.; Tang, G. A piezoelectric energy harvesting scheme based on stall flutter of airfoil section. *Eur. J. Mech. B Fluids* **2019**, *75*, 119–132. [[CrossRef](#)]
9. Wang, J.; Tang, L.; Zhao, L.; Hu, G.; Song, R.; Xu, K. Equivalent circuit representation of a vortex-induced vibration-based energy harvester using a semi-empirical lumped parameter approach. *Int. J. Energy Res.* **2020**, *44*, 4516–4528. [[CrossRef](#)]
10. Naseer, R.; Dai, H.; Abdelkefi, A.; Wang, L. Comparative Study of Piezoelectric Vortex-Induced Vibration-Based Energy Harvesters with Multi-Stability Characteristics. *Energies* **2019**, *13*, 71. [[CrossRef](#)]
11. Zou, Q.; Ding, L.; Wang, H.; Wang, J.; Zhang, L. Two-degree-of-freedom flow-induced vibration of a rotating circular cylinder. *Ocean Eng.* **2019**, *191*, 106505. [[CrossRef](#)]
12. Zhao, L.; Yang, Y. Toward Small-Scale Wind Energy Harvesting: Design, Enhancement, Performance Comparison, and Applicability. *Shock. Vib.* **2017**, *2017*, 3585972. [[CrossRef](#)]
13. Den Hartog, J.P. *Mechanical Vibrations*; McGraw-Hill: New York, NY, USA, 1956.
14. Zhao, L.; Tang, L.; Yang, Y. Comparison of modeling methods and parametric study for a piezoelectric wind energy harvester. *Smart Mater. Struct.* **2013**, *22*. [[CrossRef](#)]
15. Abdelkefi, A.; Hajj, M.R.; Nayfeh, A.H. Power harvesting from transverse galloping of square cylinder. *Nonlinear Dyn.* **2012**, *70*, 1355–1363. [[CrossRef](#)]
16. Barrero-Gil, A.; Alonso, G.; Sanz-Andres, A. Energy harvesting from transverse galloping. *J. Sound Vib.* **2010**, *329*, 2873–2883. [[CrossRef](#)]
17. Zhao, K.; Zhang, Q.; Wang, W. Optimization of Galloping Piezoelectric Energy Harvester with V-Shaped Groove in Low Wind Speed. *Energies* **2019**, *12*, 4619. [[CrossRef](#)]
18. Yang, Y.; Zhao, L.; Tang, L. Comparative study of tip cross-sections for efficient galloping energy harvesting. *Appl. Phys. Lett.* **2013**, *102*, 064105. [[CrossRef](#)]
19. Yu, H.; Zhang, M. Effects of side ratio on energy harvesting from transverse galloping of a rectangular cylinder. *Energy* **2021**, *226*, 120420. [[CrossRef](#)]
20. Qiu, J.; Liu, X.; Chen, H.; Xu, X.; Wen, Y.; Li, P. A Low-Frequency Resonant Electromagnetic Vibration Energy Harvester Employing the Halbach Arrays for Intelligent Wireless Sensor Networks. *IEEE Trans. Magn.* **2015**, *51*, 1–4. [[CrossRef](#)]
21. Kwon, S.-D.; Park, J.; Law, K. Electromagnetic energy harvester with repulsively stacked multilayer magnets for low frequency vibrations. *Smart Mater. Struct.* **2013**, *22*, 055007. [[CrossRef](#)]
22. Meeker, D. FEMM 4.2. User's Manual. Virginia 2009. Available online: <https://www.femm.info> (accessed on 29 August 2021).
23. Parkinson, G.; Smith, J. The square prism as an aeroelastic non-linear oscillator. *Q. J. Mech. Appl. Math.* **1964**, *17*, 225–239. [[CrossRef](#)]